

Estimation of latent heat flux using satellite land surface temperature and a variational data assimilation scheme over a eucalypt forest savanna in Northern Australia



Verónica Barraza^{a,*}, Francisco Grings^a, Mariano Franco^a, Vanesa Douna^a, Dara Entekhabi^b, Natalia Restrepo-Coupe^{c,d}, Alfredo Huete^c, María Gassmann^e, Esteban Roitberg^a

^a Instituto de Astronomía y Física del Espacio (IAFE-UBA-CONICET), Cdad. Universitaria, CABA, Buenos Aires, Argentina

^b Department of Civil and Environmental Engineering, Massachusetts Institute of Technology, Cambridge, Massachusetts, USA

^c School of Life Sciences, University of Technology of Sydney, Sydney, NSW, Australia

^d Department of Ecology and Evolutionary Biology, University of Arizona, Tucson, AZ, 85721, USA

^e Department of Atmospheric and Ocean Sciences, FCEyN, UBA, Piso 2, Pabellón 2, Cdad. Universitaria, C1428EGA, CABA, Argentina

ARTICLE INFO

Keywords:

Variational data assimilation
Latent heat flux
Savanna
Remote sensing

ABSTRACT

In this study, the performance of the combined-source variational data assimilation scheme (CS-VDA) is assessed in detail using *in situ* heat fluxes (i.e. sensible heat (H) and latent heat (LE)) collected at a Eucalypt forest savanna of Northern Australia (Howard Springs). The CS VDA scheme estimates surface turbulent heat fluxes via assimilation of sequences of land surface temperature (LST) and meteorological data into a surface energy balance model and a dynamic model. The main objectives of this paper were to extend previous studies to a semi-arid ecosystem and to evaluate the potential of using global meteorological forcing data (GMD) to drive the CS VDA model (rather than *in-situ* meteorological observations). In order to study the new errors associated with the use of GMD, the effects on LE of the uncertainty in air temperature and wind speed (the two key meteorological factors that controls the total estimation error) was quantitatively characterized. Using hourly *in-situ* measurements as inputs, the daily-averaged LE RMSE_{daily} was 54 W/m², which agrees with the errors previously reported in the literature. As expected, replacing local meteorological data with GMD reduces the performance of the LE estimation (GMA: RMSE_{daily} = 82 W/m², GLDAS: RMSE_{daily} = 151 W/m²). However, LE RMSE values at 8-day temporal scale for GMA are RMSE_{8-days} = 32 W/m², similar to those reported in this area for other models (MODIS (MOD16A2) and Breathing Earth System Simulator (BESS)). The error propagation analysis indicate that the CS VDA model is very sensitive to uncertainties in wind speed measurements. Moreover, there are large discrepancies between *in situ* and GMD wind speed. These two factors combined can explain the degradation in LE estimations. In this context, our study is a first step towards the characterization of an operational daily LE estimation scheme using hourly LST observations.

1. Introduction

The estimations of latent heat flux (LE) and sensible heat flux (H) are essential to understand the response and influence of vegetation to water, energy, and carbon cycle (Huntingford et al., 2005; Htley et al., 2011). Various methods have been developed using remote sensing observations to calculate surface energy fluxes at regional scale (Remote Sensing, RS), that vary from purely empirical to more physically based approaches relying on the energy balance equation (Barraza et al., 2017, 2015; Li et al., 2009; Moran and Jackson, 1991; Nagler et al., 2005; Yebra et al., 2013). Traditional approaches to estimate LE

(ET, the water vapor mass transport or evapotranspiration) from RS data rely on semiempirical relations between vegetation indexes and land surface temperature (LST) (e.g. Barraza et al., 2017, 2015; Carlson, 2007; Gillies et al., 1997; Yebra et al., 2013). For example, there is a good correlation between ET and Normalized Vegetation Index (NDVI)/LST, which require nearly simultaneous NDVI and LST data (Carlson, 2007).

Among the physically-based approaches, a number of models have been developed to estimate surface heat fluxes from RS LST observations. Many studies are based on the assimilatation of LST data using the adjoint model to evaluate the cost gradient function, and various

* Corresponding author at: Instituto de Astronomía y Física del Espacio (IAFE), CABA, Buenos Aires, Argentina.
E-mail address: vbarraza@iafe.uba.ar (V. Barraza).

kinds of land data assimilation systems have been developed (e.g. (Boussetta et al., 2008; Sabater et al., 2007)). In comparison to the empirical approaches, these models have the advantage of using temporal information to estimate a LE, and therefore to integrate all the available information in a single retrieval.

The most straightforward approach to use the model as a constraint of the estimation is to implement a variational data assimilation (VDA) scheme, which allows to combine the dynamics of the surface energy balance (SEB) models with the dynamic changes of LST to estimate LE. In this context, the VDA scheme with SEB as the physical constraint and satellite LST estimates as observations essentially finds the state that constitute a physically-possible model trajectory evolution that most closely tracks the observations.

There are two basic VDA approaches (Bateni et al., 2013; Bateni and Entekhabi, 2012; Xu et al., 2014): (1) combined-source scheme (CS) (not distinguishing the difference between soil and canopy temperatures), and (2) the dual-source (DS) scheme (accounts for the difference between soil and canopy temperatures and considers the interactions between them). These schemes were tested at two grassland sites (Bateni et al., 2013; Bateni and Entekhabi, 2012) and over six FluxNet sites with different vegetation covers (grassland, cropland, and forest) and climate conditions over USA (Xu et al., 2014).

In this study, the performance of the CS VDA framework is assessed in detail using surface heat fluxes collected at a Eucalypt forest savanna of Northern Australia. We implemented the CS variant of the VDA scheme, because Xu et al. (2014) found that surface energy fluxes estimated by CS and DS VDA models do not show significant differences over forested areas. Australian savannas are ecologically intact at large scales with low levels of fragmentation, providing an ideal location to study this retrieval scheme in an open forest environment. Specifically, our aim is to evaluate the robustness of CS VDA scheme over a savanna ecosystem that is primarily driven by water availability, and in which vegetation exerts a strong control over transpiration. As benchmark, we compared our LE estimations with others LE RS products, like MOD16A2 (Mu et al., 2007) and Breathing Earth System Simulator (BESS) (Jiang and Ryu, 2016; Ryu et al., 2011). These product are global remote sensing evapotranspiration products with a temporal resolution of 8-days, that use as input auxiliary information like global meteorological data (GMD), derived from a reanalysis dataset, providing global spatial information to generate an operative product. On the contrary, the CS-VDA model is typically implemented using *in situ* meteorological data as input (Bateni et al., 2013; Bateni and Entekhabi, 2012). Therefore, as a second objective, we also evaluated the ability of the CS-VDA to estimate LE using global meteorological data (instead of *in-situ* data) as input.

For this analysis, we have addressed the following questions: 1) How much variance of the observed LE can be explained by the CS VDA model?; 2) Is it possible to monitor the seasonal dynamics of LE at the Eucalypt forest savanna?; 3) How is the performance of CS VDA model when using *in-situ* meteorological data and remotely sensed LST as input?; And finally, 4) How much does this performance degrade when using GMD and LST remote sensing as input?.

2. Methodology

2.1. Site description and *in situ* eddy covariance measurements

To run the VDA model we used as inputs water vapor fluxes and meteorological measurements from an eddy covariance (EC) site located at Howard Springs (AU-Hsp) ($12^{\circ} 30'S$, $130^{\circ} 45'E$, Elevation is close to 64 m), humid zone of the Northern Territory, Australia. The AU-Hsp eddy flux tower is located in the Black Jungle Conservation Reserve, an open woodland savanna dominated by an under-story of annual grasses and two overstory tree species: *Eucalyptus miniata* and *Eucalyptus tetrodonta* (Hutley et al., 2011; Kamiah et al., 2011). This site is characterized by a wet season from December to March and

accounts for more than 90% of the 1750 mm mean annual precipitation. This is followed by a dry season (May to September) (Taylor and Tulloch, 1985).

We used the OzFlux standard processing protocol OzFluxQC v2.7.1 released under the GNU general public license (2007) by the OzFlux community using Python (Enthought Python Distribution version 7.3-1) (Isaac et al., 2017). The data processing included removal of spikes, rejection of fluxes where more than 1% of 10 Hz observations were missing from the 30-minute average, linear corrections for sensor drift and calibration changes, WPL and other corrections, and rejection of observations when wind originated from behind the 3D-anemometer and tower. The resulting half-hourly EC measurements were post-processed to ensure consistency among sites and to reduce uncertainties in the computed fluxes: this included additional quality control assessment and removal of outliers (Restrepo-Coupe et al., 2015, 2013).

The instrument mast is 23 m tall on a canopy of 14 m. Heat, water vapor and carbon dioxide measurements were taken using the open-path eddy flux technique. Temperature, humidity, wind speed, wind direction, rainfall, incoming and reflected shortwave radiation and net radiation were measured above the canopy. Turbulent fluctuations of wind speed and air temperature were measured with a Campbell Scientific (Logan, UT) 3-D sonic anemometer (model CSAT3) and water vapor concentration was measured with a Campbell Scientific fast-response krypton hygrometer (model KH20). Above canopy CO₂ concentration were measured with open path IRGA (LI-7500).

Fluxes and meteorological variables used in this study and measured at Howard Springs location were: latent heat flux (LE, W/m²), air temperature (Ta, °C), daily precipitation (Prec, mm), relative humidity (RH, %), shortwave incoming radiation (SW down, W/m²), longwave incoming radiation (LWdown, W/m²), sensible heat flux (H, W/m²), net radiation (Rn, W/m²), wind speed (U, m/s), and atmospheric pressure (kPa).

2.2. Surface energy balance (SEB) model

The CS VDA model is presented in detail in Bateni et al. (2013) and Bateni and Entekhabi (2012). In this section we summarize the model. The CS VDA model considers one layer (soil and vegetation as a single source), so the surface energy balance equation can be expressed as

$$R_n = H + LE + G \quad (1)$$

where R_n is net radiation (W/m²), H is sensible heat flux (W/m²), LE is latent heat flux (W/m²), and G accounts for both the ground heat flux and the energy stored in the canopy (W/m²) (Oke, 1988). H is modeled as follows:

$$H = \rho c_p C_H U (T - T_A) \quad (2)$$

where ρ is the air density (kg/m³), c_p is the air specific heat at constant pressure (1006 kJ/kg K), U is the surface mean wind speed (m/s), T_A is the air temperature (K) at a reference height, and C_H is the bulk heat transfer coefficient. C_H can be written as the product of the neutral bulk heat transfer coefficient (C_{HN}) and a correction function for atmospheric stability, f (R_i) (where R_i is the bulk Richardson number). C_{HN} can be related to roughness length scales for heat and momentum (Liu et al., 2008), and it is mainly a function of vegetation phenology and is assumed to vary on a monthly temporal scale (Bateni et al., 2013; Crow and Kustas, 2005; Jensen and Hummelshøj, 1995; McNaughton and Hurk, 1995; Xu et al., 2014).

$$C_H = C_{HN} * f(R_i) = C_{HN} * (1 + 2(1 - e^{10R_i})) \quad (3)$$

R_i is estimated by:

$$R_i = g/(T_{pot}) * \Delta T_{pot} \Delta z / (\Delta U)^2 \quad (4)$$

where g (m/s²) is gravitational acceleration, T_{pot} (K) is the air potential temperature (Bohren and Albrecht, 1998), z (m) is vertical height, and Δ represents the differences across height differences Δz .

The second parameter is evapotranspiration fraction (EF), which scales the energy partition between the turbulent heat fluxes and is given by

$$EF = LE / (Rn + G) = LE / (H + LE) \quad (5)$$

EF is introduced to calculate LE as:

$$LE = H (EF / (1 - EF)) \quad (6)$$

2.3. The heat diffusion equation

In the CS VDA model the one-dimensional heat diffusion equation (Eq. (7)) is used to model terrain thermal inertia. In general, for open vegetation (like our study site), it is assumed that all the thermal inertia of the terrain is provided by the soil. Therefore, we are interested in model the temperature profile within the soil column as,

$$c \frac{\partial T(z, t)}{\partial t} = p \frac{\partial^2 T(z, t)}{\partial z^2} \quad (7)$$

where c is the soil volumetric heat capacity ($J / m^3 K$) and p is the soil thermal conductivity ($W/m K$). For simplicity, in this study, the soil temperature at the surface, $T(z = 0, t)$, is written as $T(t)$.

To solve the heat diffusion equation, boundary conditions at the top and the bottom of the soil column are needed. The top boundary condition, $T(z = 0, t)$, is retrieved from the surface boundary forcing equation $-p dT(z = 0, t) / dz = G(t)$. At the bottom boundary, a Neumann boundary condition is used, which pointed out that at a depth l where the heat wave have disappeared:

$$\frac{\partial T(l, t)}{\partial z} = 0 \quad (8)$$

Where l is set at 0.5 m (Bateni et al., 2013; Hu and Islam, 1995).

2.4. Adjoint state formulation

The two parameters that should be estimated by the VDA approach are C_{HN} and EF. As was mentioned previously, C_{HN} varies on a monthly time scale ($N = 30$ days), however EF can vary from day to day. The assumption of the CS- VDA model are: constant monthly C_{HN} , daily constant EF, constant p and c during the modeling period, and EF limitations to an upper bound of 0.97 and lower bound of 0.1 to avoid numerical instabilities. A cost function (J) is defined to retrieve the unknown parameters by minimizing the differences between the LST observations and estimations. The cost function can be written as:

$$\begin{aligned} J(T, R, EF, \lambda) = & \sum_{i=1}^N \int_{t_0}^{t_1} [T_{obs,i}(t) - T_i(t)]^T K_T^{-1} [T_{obs,i}(t) - T_i(t)] \partial t \\ & + (R - R')^T K_R^{-1} (R - R') \\ & + \sum_{i=1}^N (EF_i - EF'_i)^T K_{EF}^{-1} (EF_i - EF'_i) \\ & + 2 \sum_{i=1}^N \int_{t_0}^{t_1} \int_0^l \lambda_i(z, t) \left[\frac{\partial T(z, t)}{\partial t} \right. \\ & \left. - D \frac{\partial^2 T(z, t)}{\partial z^2} \right] \partial z \partial t \end{aligned} \quad (9)$$

The first term in the cost function represents the square of the fitting errors between the observed ($T_{obs}(t)$) and measured ($T(t)$) LST observations. R is a function of C_{HN} ($C_{HN} = \exp(R)$), chosen to make C_{HN} always positive and physically meaningful. Primed parameters (EF' and R') are prior estimates of EF and R. Therefore, the second and third terms penalize large deviations from the prior values. The last term is the heat diffusion equation, which is adjoined to the model via the lagrange multiplier, K_T^{-1} , K_R^{-1} , and K_{EF}^{-1} are the numerical constant parameter that weigh each term in the cost function and control its rate of convergence. Following (Bateni et al., 2013) these factors are set to

$K_T^{-1} = 0.01$, $K_R^{-1} = 1000$, and $K_{EF}^{-1} = 1000$, which are very flat priors for R and EF. The daily assimilation window goes from 9:00 to 16:00 LT ($\tau_0 = 9$ and $\tau_1 = 16$). The assimilation periods are arranged in 30-day blocks ($N = 30$).

The optimal values of R and EF are obtained by minimizing the cost function J . To this aim, its first variation should be set to zero. This leads to a number of Euler-lagrange equations that should be solved simultaneously through and iterative loop to obtain optimal values of CHN and EF. These equations and further details can be found in Bateni et al., 2013.

2.5. Land surface temperature data sets

LST products were provided by Copernicus Global Land Service at <http://land.copernicus.vgt.vito.be/PDF/portal/Application.html#Home>. LST data set were generated from sensors onboard different geostationary (GEO) satellites. The product presents a spatial resolution of 0.05°. The period analyzed was 2010–2015. For the study area, the GEO satellites used to calculate the LST product were Multi-Function Transport Satellite (MTSAT, from 2010 to 2014) and Himawari (from 2015). The product used the split-window algorithm to generate the LST product. For more information about the algorithm see <http://land.copernicus.eu/global/products/lst>.

The CS VDA model provided hourly estimations of the energy components (Eq. (1)). Even though the calculations are hourly, its assimilation is on a daily window. Based on this, there were uncertainties associated to hourly LST and EC time series that should be analyzed with the aim to provide better EF estimations. Firstly, the presence of gaps in the LST time series due to cloud coverage should be evaluated. Temporal filling of unreliable LST data as well as smoothing filters can greatly improve the accuracy of inputs. However, the filled values are interpolations. In this context, we have tested when it was possible to fill the hourly LST dataset without introducing much error in estimated LE values. When the gaps in the LST time series occur from 10 to 14 hs (i.e. when the LST variation is smoother), the uncertainties in the values used for filling the dataset do not introduce significant errors to the model and thus the completion of the time series is reliable. On the other hand, the model is very sensitive to variations in the LST at the beginning and the end of the assimilation window. For this reason, the days in which the missing values correspond to one of both contours of the assimilation window were excluded from the LST series. Based on this criteria, we produced a new filtered LST time series to be used as input in the CS VDA model.

EC method delivers continuous data sets of mass and energy exchange between ecosystem and atmosphere. However, gaps due to unfavorable micro-meteorological conditions and due to instrument failure are inherent in the data stream. We made a similar analysis to the LST time series and found equivalents results. Daily EC dataset were excluded when missing values were found immediately before of the initial/end of the assimilation window.

2.6. Global meteorological data sets

In this study, we evaluated the performance of the CS VDA model using as input forcing data provided by two different global meteorological datasets (GMD): the Modern Era Retrospective-analysis for Research and Applications (GMA/MERRA) reanalysis data from coupled land surface models (Schubert et al., 1993) and with the Global Land Data Assimilation System (GLDAS/NOAH, temporal composition: 3 h) LSM forced off-line (Rodell et al., 2004). Specifically, the *in situ* observations were replaced by GMD (Table 1) estimations for this six input variables:

- wind speed (U , m/s),
- air temperature (T_a , K),
- atmospheric pressure (P , kPa),

Table 1

Summary of the Spatial and Temporal Resolution of the products used in this analysis.

	Spatial Resolution	Temporal Resolution
In situ	1 km	hourly
LST	0.05°	hourly
GMA/MERRA	0.03 ° x 0.5 °	hourly
GLDAS/NOAH	0.25° × 0.25°	3 hours

- air relative humidity (RH),
- short wave incoming radiation (SWdown, W/m²),
- long wave incoming radiation (LWdown, W/m²)

When we used GMD in the CS-VDA model all the products (Table 1) were resampled to a spatial resolution of 25 km that extended a period from 2009 to 2015.

2.7. Evaluation seasonal analysis

In order to analyze the performance of the EF retrieval, it is interesting to find some natural constraints to LE in the study area. In this context, it is well known that surface conductance (G_s) plays an active role in limiting LE (Monteith, 1985). G_s is in itself a function of vegetation and environmental variables, including Ta, vapor pressure deficit (VPD), soil and leaf water potential, and photosynthetically active radiation (PAR) (Allen et al., 1998; Monteith, 1985). To understand the main drivers of the seasonal cycle of EF, we compared CS-VDA estimations with extreme EF values calculated using extreme values of G_s (minimum and maximum, denoted as EF fn ($G_{s\min}$) and EF fn ($G_{s\max}$)).

To estimate G_s , we used *in-situ* meteorological and EC data and the Penman-Monteith (PM)-equation:

$$G_s = \left[\frac{G_a}{\varepsilon \cdot A - (\varepsilon + 1) + \left(\frac{G_a c_p \cdot \rho [e_s(Ta) - e_a]}{\gamma} \right)} \right] \quad (10)$$

where e_a is the actual vapour pressure (kPa); e_s is the saturation vapour pressure (kPa); γ is the psychrometric coefficient (kPa/°C); ρ is the mean air density (kg/m³); c_p is the specific heat of air at constant pressure (J/kg K); A is the available energy absorbed by the surface (net absorbed radiation minus soil heat flux) (W/m²); G_s is the surface (m/s) and G_a is the aerodynamic conductance (m/s) and $\varepsilon = s/\gamma$; where s is the slope of the saturation vapour pressure versus temperature curve (kPa/°C). In Appendix A there are more information about the derivation of G_a .

Next, we need to calculate EF using the estimated extreme values of G_s (minimum and maximum, denoted as EF fn ($G_{s\min}$) and EF fn ($G_{s\max}$)). To this end, we used the PM-equation to calculate LE and then EF using *in-situ* meteorological and EC data,

$$LE = \left[\frac{\varepsilon \cdot A + \left(\frac{c_p \cdot \rho}{\gamma} \right) [e_s(Ta) - e_a] \cdot G_a}{\varepsilon + 1 + \left(\frac{G_a}{G_s} \right)} \right] \quad (11)$$

2.8. Evaluation metric

To evaluate the relationship between LE estimations and observations (based on EC observations), we obtained the coefficient of determination (r^2), correlation coefficient (r), the root mean square error (RMSE) and the mean bias error (BIAS). We calculated these evaluation metrics at daily and 8-days' time scale. Since there are spatial scale inconsistencies between satellite and *in-situ* data ((i) eddy covariance fluxes and meteorological sensors (radiation, temperature, humidity) have different footprints and (ii) the tower flux footprint is only a small

fraction of the remote sensing pixel), we dealt with them using Type II regressions,

$$RMSE = \sqrt{\frac{\sum_{i=1}^N (P_i - O_i)^2}{N}} \quad (15)$$

$$BIAS = \frac{\sum_{i=1}^N (P_i - O_i)}{N} \quad (16)$$

where P_i is model-predicted value, O_i is observed value and N is number of observations. The average daily surface flux value was calculated only in the assimilation window (9:00–16:00 LT), so N was equal to 8. To compare with literature and others RS product, average 8-days LE values were calculated. In particular, we compared the 8-days CS-VDA results with MODIS (MOD16A2) and Breathing Earth System Simulator (BESS) LE product.

The official MOD16A2 product is based on the Penman-Monteith (PM, Eq. (11)) equation and uses daily meteorological reanalysis data (air temperature, and vapor pressure deficit) and 8-day remotely sensed vegetation property dynamics (MOD15 leaf area index product) to estimate G_s and other key environmental drivers (Mu et al., 2007). The BESS is a concise process-based model used to estimate carbon and water fluxes at global scale (Jiang and Ryu, 2016). The BESS products use MODIS atmosphere (Collection 6) (MOD(Y)D04_L2, MOD(Y) D05_L2, MOD(Y)D06_L2, MOD(Y)D07_L2) and land (Collection 5) products (MOD(Y)D11_L2, MCD12Q1, MCD15A2, MCD43B2, MCD43B3), others satellite datasets (Polarization and Directionality of the Earth's Reflectances, POLDER 3(Chen et al., 2005)), four variables from reanalysis datasets (NCDEP/NCAR Reanalysis 1 data (Surface Flux) (Kalnay et al., 1996)), and three ancillary datasets as input data (Köppen-Geiger global climate classification map (Kottek et al., 2006; Ryu et al., 2011)).

2.9. Uncertainties analysis

An uncertainty analysis was performed to understand the effect of replacing *in-situ* meteorological data with reanalysis GMD data. In addition to the errors in the main assimilated variable (e.g., LST), any errors in the forcing inputs will propagate through the model and affect the final estimates of EF. We consider the sensitivity of an estimate of EF, calculated using the CS-VDA model to changes in a parameter or input data variable, p_i where in general:

$$F = f(p_1, p_2, p_3, \dots, p_n) \quad (17)$$

where n is the number of parameters and input data variables. Then:

$$F + \Delta F = f(p_1 + \Delta p_1, p_2 + \Delta p_2, p_3 + \Delta p_3, \dots, p_n + \Delta p_n) \quad (18)$$

Expanding Eq. (12) in Taylor series and retaining only the terms of first order:

$$\Delta F = \left| \frac{\partial F}{\partial U} \right| \cdot \Delta U + \left| \frac{\partial F}{\partial Ta} \right| \cdot \Delta Ta + \left| \frac{\partial F}{\partial P} \right| \cdot \Delta P \quad (19)$$

where U is wind speed (m/s), Ta is air temperature (K) and P is atmospheric pressure (kPa), ΔF represent the total error of the EF and the differentials $\partial F / \partial p_i$ define the sensitivity of the estimate to each parameter or variable and were derived theoretically from the functional relationship previously presented in Section 2.2, 2.3 and 2.4 and evaluated using the observed data. ΔU , ΔTa and ΔP correspond to the errors of U , Ta and P with respect to the *in situ* measured values. Assuming that all parameters p_i are uncorrelated, we calculated the error in EF as the square terms sum of Eq. (18).

$$\Delta F = \sqrt{\left(\frac{\partial F}{\partial U} \right)^2 \cdot \Delta U^2 + \left(\frac{\partial F}{\partial Ta} \right)^2 \cdot \Delta Ta^2 + \left(\frac{\partial F}{\partial P} \right)^2 \cdot \Delta P^2} \quad (20)$$

In this analysis, a number of tests were performed to understand the impact of the uncertainties on the estimate of the turbulent surface

Table 2

Summary of the relationship between daily-averaged observed (Copernicus product) and estimated (CS VDA) LST (K).

Month	RMSE (K)					
	2010	2011	2012	2013	2014	2015
Jan	–	–	4.35	–	2.76	–
Feb	–	–	3.07	5.16	–	3.39
Mar	–	–	2.65	5.24	2.83	3.42
Apr	–	3.60	2.52	3.27	2.63	2.85
May	–	2.78	3.39	3.23	1.65	3.34
Jun	2.88	–	5.53	4.21	2.17	2.35
Jul	3.15	–	5.60	4.41	2.49	2.39
Aug	3.06	3.45	5.92	2.71	3.27	2.57
Sep	3.22	3.25	6.25	2.90	3.30	–
Oct	4.23	4.20	5.83	2.88	3.30	–
Nov	3.28	3.99	5.49	–	3.40	2.45
Dec	–	–	5.34	3.38	–	2.29

Table 3

Summary of the relationship between estimated and observed daily average LE (W/m^2) from January to December for the study period (2010–2015) (– is not data available).

Month	2010 LE - RMSE (W/m^2)	2011 LE - RMSE (W/m^2)	2012 LE - RMSE (W/m^2)	2013 LE - RMSE (W/m^2)	2014 LE - RMSE (W/m^2)	2015 LE - RMSE (W/m^2)
Jan	–	–	172.75	–	51.21	–
Feb	–	–	209.27	190.83	–	88.26
Mar	–	–	212.57	190.06	77.52	84.28
Apr	–	96.81	236.28	98.89	81.77	78.00
May	–	98.74	193.93	75.19	69.50	45.86
Jun	45.20	–	180.26	54.64	64.70	49.14
Jul	93.49	–	158.34	54.65	63.17	38.17
Aug	61.57	102.54	156.89	46.52	72.52	47.22
Sep	90.05	95.44	157.92	57.05	74.65	–
Oct	108.61	115.62	210.69	53.41	77.96	–
Nov	106.74	98.96	225.71	–	85.71	48.25
Dec	–	–	223.37	56.16	–	63.64

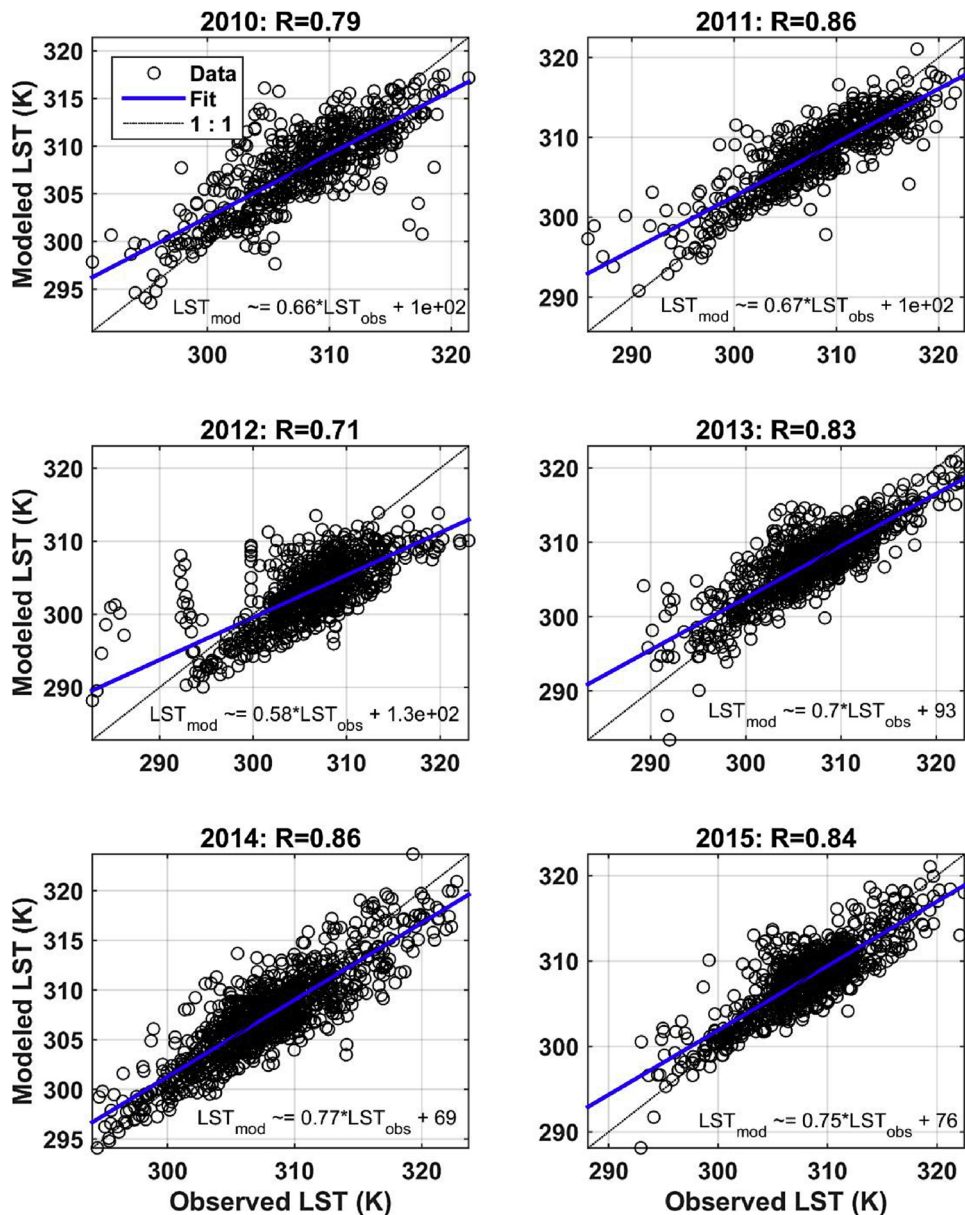


Fig. 1. Relationship between observed (LST_{obs}) (Copernicus product) and estimated (LST_{mod}) (CS VDA) LST for the 2010–2015 period.

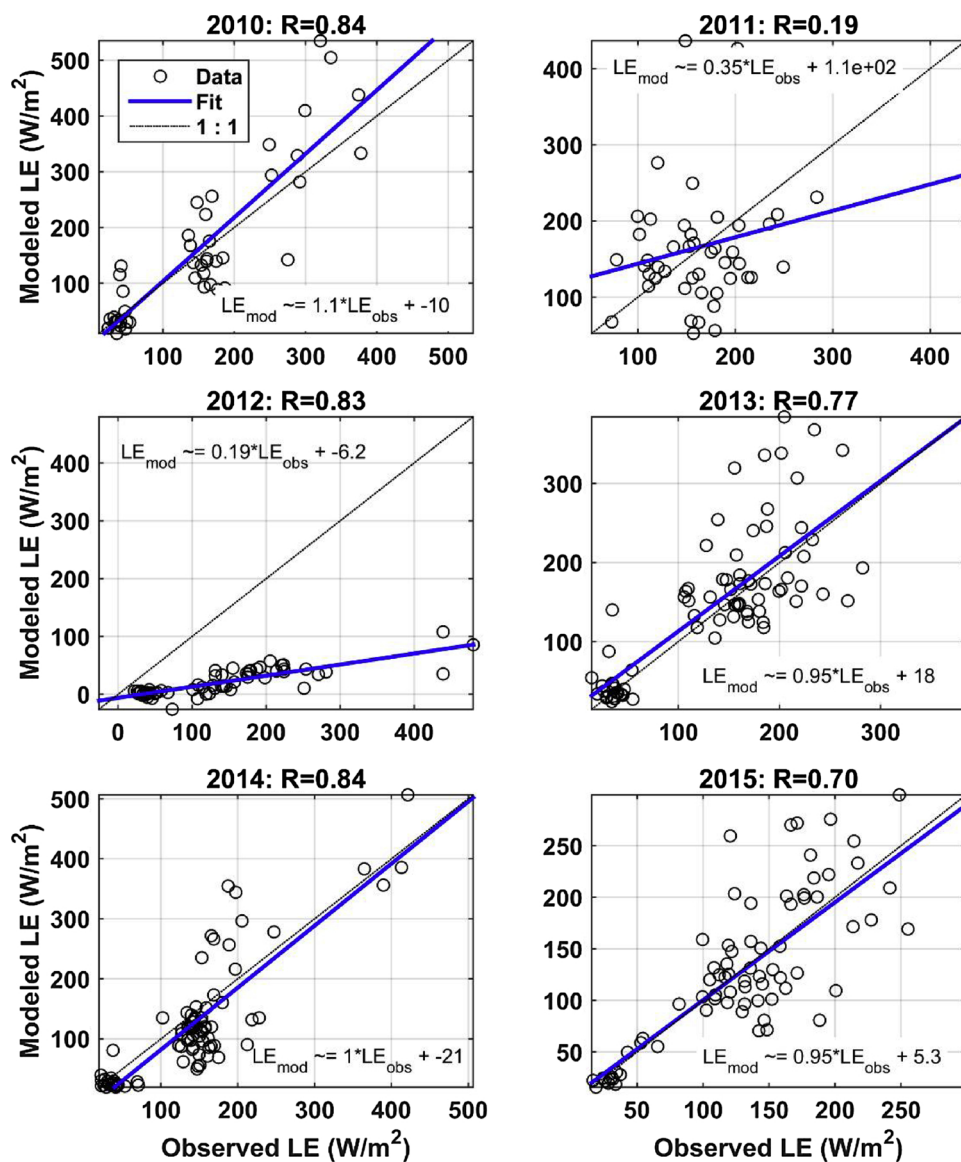


Fig. 2. Relationship between observed (LE_{obs}) and estimated (LE_{mod}) daily average LE (W/m^2) for the 2010–2015 period.

Table 4

July to November summary of the relationship between observed and estimated daily average EF, LE (W/m^2) and H (W/m^2).

Jul- Nov Period	EF			LE (W/m^2)			H (W/m^2)			n
	BIAS (W/m^2)	RMSE (W/m^2)	r^2	BIAS (W/m^2)	RMSE (W/m^2)	r^2	BIAS (W/m^2)	RMSE (W/m^2)	r^2	
2010	0.15	0.18	0.27	-40.61	-72.59	0.65	53.52	70.66	0.72	64
2011	0.22	0.24	0.14	41.25	68.63	0.69	77.12	99.77	0.67	50
2012	0.07	0.09	0.27	119.43	130.23	0.21	60.97	74.78	0.63	40
2013	0.12	0.14	0.49	31.82	46.84	0.81	31.17	41.86	0.80	50
2014	0.16	0.18	0.43	30.34	47.11	0.73	48.05	66.09	0.85	56
2015	0.12	0.15	0.35	28.24	34.98	0.73	31.52	71.22	0.75	28
Total (excluded 2012)	0.15	0.17	0.33	34.45	54.03	0.70	48.28	69.92	0.70	248

fluxes for several key input variables. The variables studied were selected as the ones that presented the greater $\partial EF / \partial pi$ mean values. The effect of the variation of P on ΔEF has been proved to be negligible in comparison to those of U and Ta, and so the third term has been disregarded.

3. Results

3.1. Comparison of estimated land surface temperature to remote sensing observations

In general, the CS VDA model presented a good fit in terms of LST RMSE at AU-Hsp at daily time scale (assimilation windows) during the study period (Table 2 and Fig. 1). In particular, CS VDA model

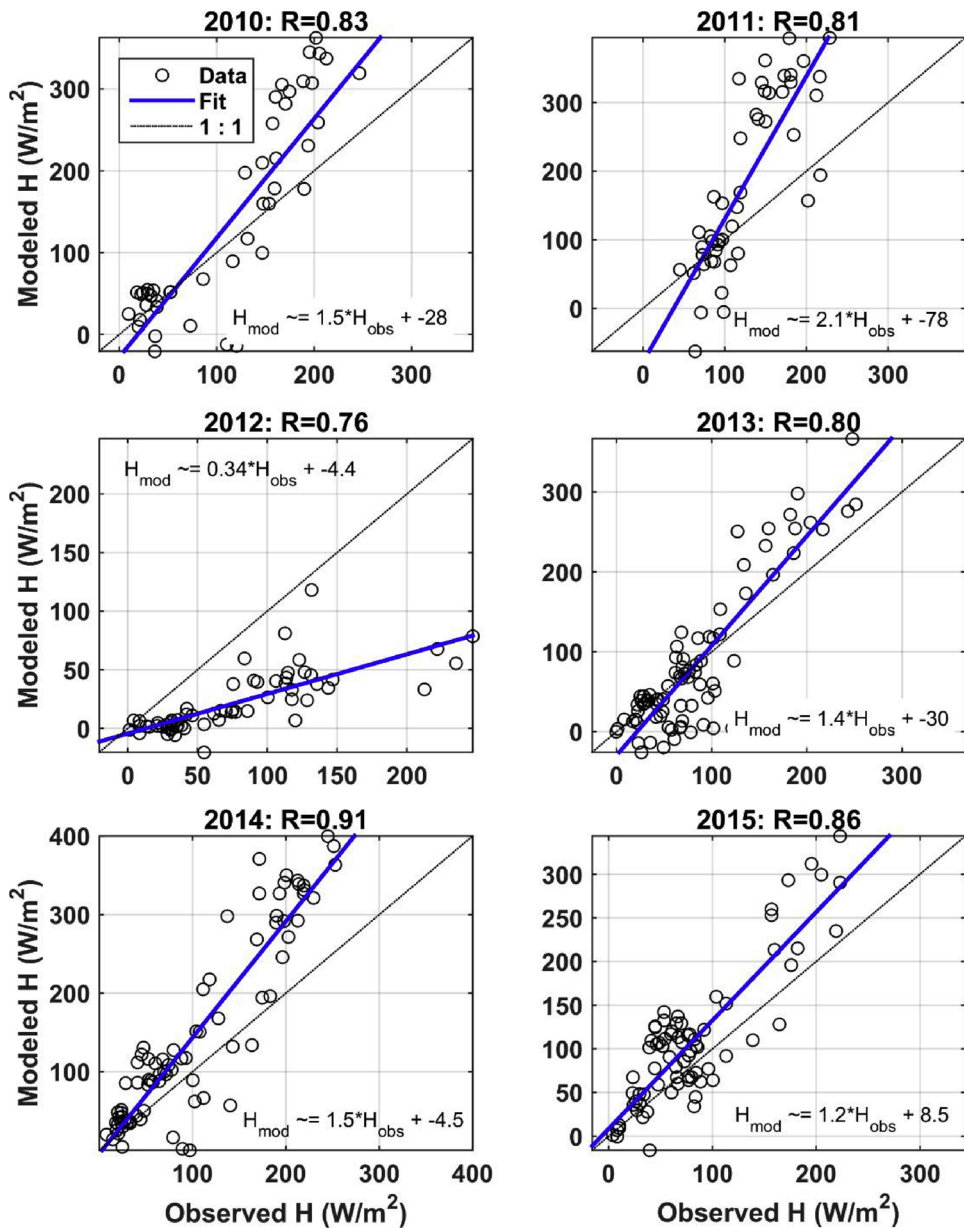


Fig. 3. Relationship between observed (H_{obs}) and estimated (H_{mod}) daily average H (W/m^2) for the 2010–2015 period.

explained more than 80% of LST variance ($p < 0.05$) with RMSE lower than 3.6 K for 2010, 2014 and 2015.

3.2. Comparison of estimated surface fluxes to *in situ* EC observations

CS VDA model presented good performance at AU-Hsp for almost all the study period (excluded 2012) (Table 3). In particular, CS VDA model explained more than 70% of the variance at LE ($p < 0.05$) with RMSE lower than 100 W/m^2 . This error is large when compared with typical approaches, but we need to consider that this is a daily product. For 2012, the CS VDA model systematically underestimate LE and this led to the highest RMSE value in the time series ($> 200 \text{ W}/\text{m}^2$). Fig. 2 and Table 4 shows the relationship between surface fluxes (LE and H) estimated using CS VDA model and EC observations during July and November (data was available during these months in the whole period). The daily average LE and H presented a mean RMSE of 54 and 68 W/m^2 , respectively with a mean BIAS of 34 and 48 W/m^2 , respectively. We also calculated the 8-days temporal composition of LE, which presented a RMSE of 22 W/m^2 , a value which is of the order of the

typical approaches based on RS estimations. As has been discussed previously, the best performance was obtained for 2014 and 2015; and the worst for 2012. This was related to higher RMSE errors found in LST estimations. This error is also shown in H and EF estimations that depend on estimated LST (Fig. 2–4). This was analyzed in detail in the discussion section.

As explained earlier, in order to study the soundness of the seasonal cycle of estimated EF, we computed extreme values of EF using constant surface conductance (G_s) values (minimum and maximum, denoted as $\text{EF}(G_{\text{smin}})$ and $\text{EF}(G_{\text{smax}})$ respectively). As can be seen in Fig. 5, the estimated values of EF are always lower than $\text{EF}(G_{\text{smax}})$ and higher than $\text{EF}(G_{\text{smin}})$ (the shaded grey areas show the annual variation of the estimations). The lowest values of estimated EF were observed in August (dry season from April to September), and the maximum in February, during the rainy season. Therefore, the temporal dynamic of estimated EF was generally reasonable. In particular, the seasonal variation of EF is very well captured in the transient periods and during the growing season. However, the model underestimates EF from June to December (with the largest differences in August).

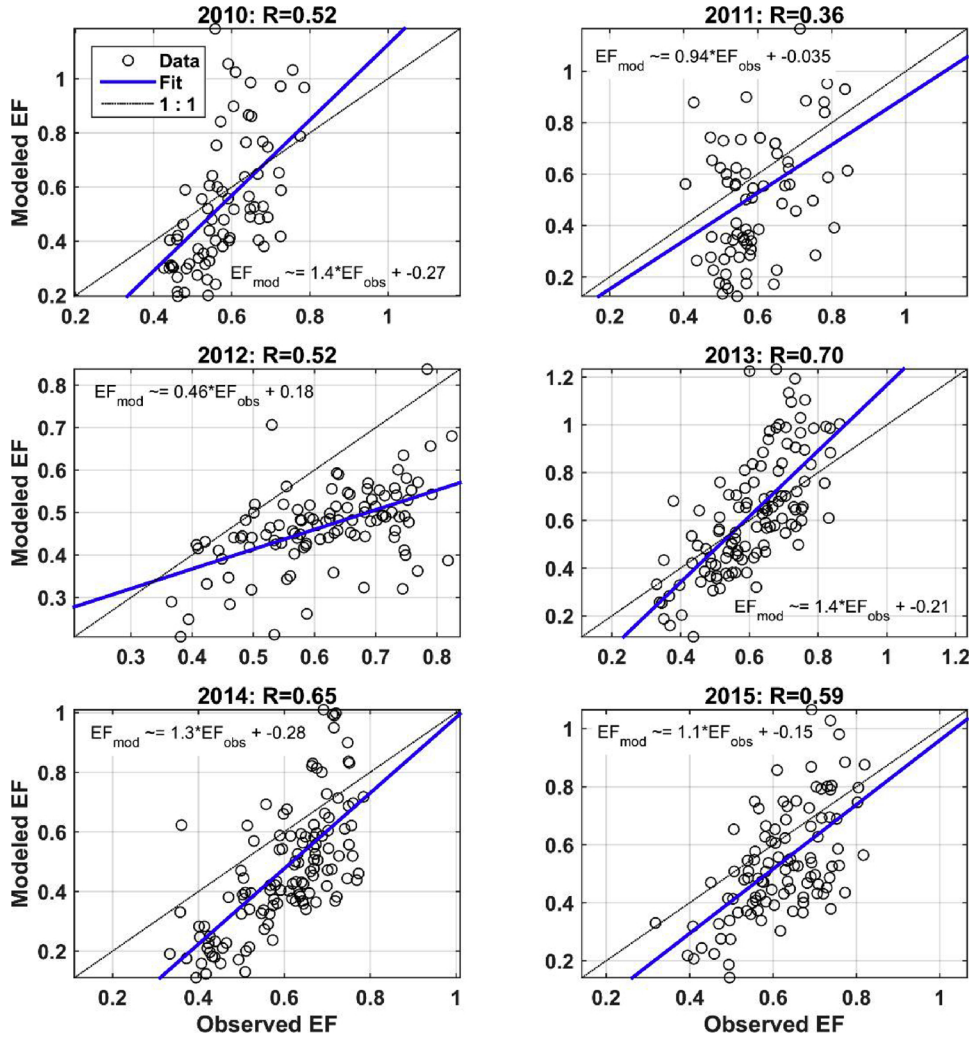


Fig. 4. Relationship between observed (EF_{obs}) and estimated (EF_{mod}) daily average EF for the 2010–2015 period.

3.3. Global Meteorological Dataset as CS VDA input

In this section we will study the degradation of the EF estimation when *in situ* ancillary information is replaced with GMD data (specifically, we have replaced U, Ta, P, RH, SWdown, LWdown). To operationalize the VDA scheme using GMD data, two sources of degradation need to be studied: (1) measured vs modeled *in situ* variables and (2) hourly step vs 3-hours data (the temporal resolution of GMA/MERRA and GLDAS is 1 and 3-hourly, respectively). In order to achieve this goal, in Table 5 we compared the daily-averaged RMSE for four different input datasets: hourly *in situ* dataset (benchmark case), 3-hours *in situ* dataset, hourly GMD dataset (GMA/MERRA) and 3-hours GMD dataset (GLDAS). As it can be seen at Table 4 the performance of the CS VDA scheme with hourly or 3-hours dataset is similar for the study site. However, we found that replacing local meteorological data with global meteorological data reduce the performance of the LE model at the study area, for both GMA/MERRA ($RMSE_{daily} = 80.70 \text{ W/m}^2$) and in special for GLDAS ($RMSE_{daily} = 151.87 \text{ W/m}^2$). In spite of this, it is important to mention that when moving to 8-day temporal scale, GMA/MERRA: $RMSE_{8\text{-days}} = 32.20 \text{ W/m}^2$. This value is similar to those obtained at the study area by other products (MOD16A2: 31.14 W/m^2 and BESS: 41.40 W/m^2).

3.4. Uncertainty analysis

Finally, an error propagation analysis was performed to evaluate the

impact of the uncertainties in the input meteorological variables on the surface turbulent heat flux estimates using the CS VDA scheme. Firstly, we have evaluated to which variables corresponded the larger terms of Eq. (18). We found that the air temperature (Ta) and the wind velocity (U) dominate by far the total EF error. Therefore, we proceed to evaluate the discrepancies (Δ) between observed (*in situ*) and estimated (by GMA (MERRA) or GLDAS) values of these variables. Results are shown in Fig. 6. In general, the relations ranges from noisy (for P and T) to poor for U. Therefore, it is expected that these discrepancies should introduce errors in estimated EF. It is worthwhile to mention than for these variables in this study site, GMA (MERRA) presented a better estimations than GLDAS.

Given these errors in the key input variables, we can now estimate the error in EF (ΔEF) using Eq. (18). To this end, we need to compute $\partial EF / \partial p_i$ for every key variable. Results are shown in Figs. 7 and 8. As expected, EF error increase with both ΔU and ΔTa ; but it presented a proportional relation with U and an inversely proportional with Ta. The larger errors are by far related to the $|\Delta EF / \Delta U| |\Delta U|$ term, for which moderate mismatches between *in situ* and modeled values of U (for example, $\Delta U = 3 \text{ m/s}$) leads to a $\Delta EF > 1$ for moderate mean values of U ($U > 1.5 \text{ m/s}$). Since EF is by definition in the range [0, 1], the retrieval in this condition will be useless. When varied together both variables, U and Ta, (Figs. 7 and 8) the estimated EF from the CS scheme were less sensitive to the uncertainties in Ta than in U. The model is also more sensitive to the uncertainties in Ta and U for lower Ta values ($< 310 \text{ K}$) and for higher U values ($> 1.5 \text{ m/s}$).

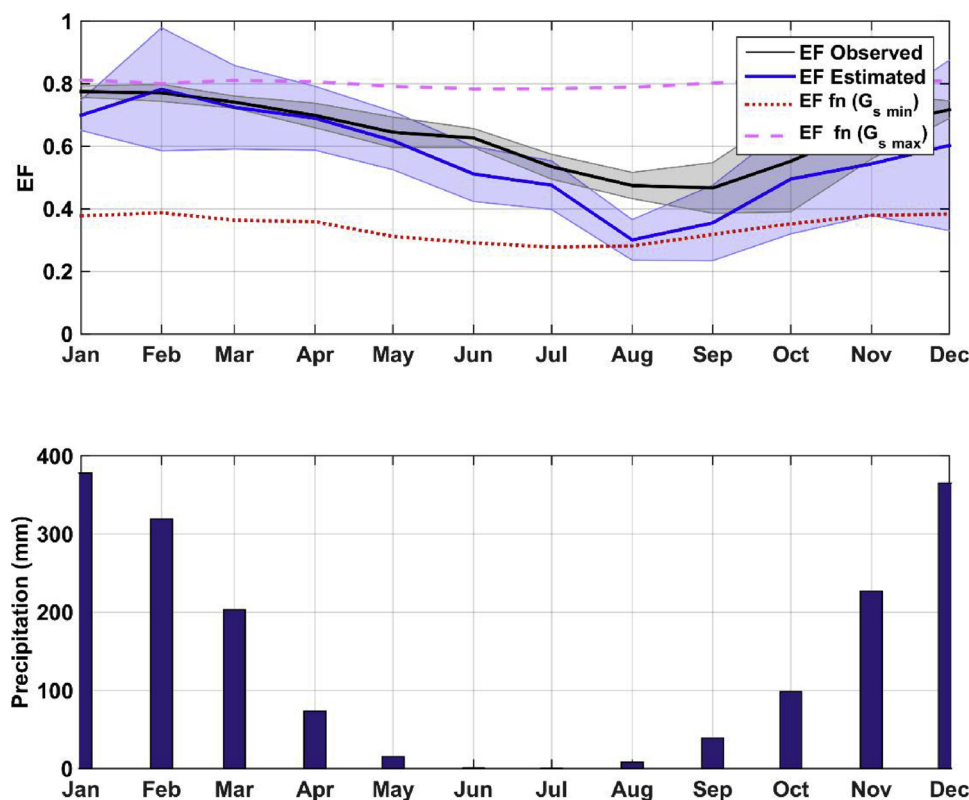


Fig. 5. Time series of average monthly estimated and observed evapotranspiration fraction (EF) derived from the CS VDA model and EF obtained using extreme values of G_s (minimum and maximum, denoted as EF ($G_{s\min}$) and EF ($G_{s\max}$) respectively) (Upper panel), and average monthly precipitation (mm) (Lower panel).

Table 5

Summary of daily-averaged LE RMSE (observed vs estimated) for four different inputs: hourly in situ dataset (benchmark case), 3-hours in situ dataset, hourly GMD dataset (GMA/MERRA) and 3-hours GMD dataset (GLDAS).

Meteorological input	Meteorological data			
	In-situ dataset		GMD (GMA/MERRA)	GMD (GLDAS)
	hourly RMSE (W/m ²)	3-hour RMSE (W/m ²)	hourly RMSE (W/m ²)	3-hour RMSE (W/m ²)
2010	62.17	60.28	88.43	167.57
2011	73.40	67.13	102.90	161.91
2012	142.55	148.47	142.36	171.13
2013	46.79	45.53	90.28	149.08
2014	52.82	54.03	72.21	153.81
2015	42.07	45.71	61.70	135.14
Total	75.85	76.70	94.5	155.07
Total (excluded 2012)	54.36	53.39	80.70	151.87

4. Discussions and conclusions

In this study, satellite LST observations were assimilated into a VDA scheme, which treats the soil and vegetation as one medium. The unknown parameters were daily EF and monthly neutral bulk transfer coefficient (C_{HN}). The EF estimates were in agreement with the observations in terms of magnitude and seasonal dynamics. We extended previous studies (Bateni et al., 2013; Bateni and Entekhabi, 2012; Castelli et al., 1999; Xu et al., 2014) to a semi-arid ecosystems, in which EF presented a different seasonal behavior.

Furthermore, in order to move towards operationalization, we tested the VDA scheme using global meteorological forcing data rather than site-specific observations. In contrast to previous studies (Bateni et al., 2013; Bateni and Entekhabi, 2012; Xu et al., 2014) that used half-

hour *in situ* meteorological data and satellite LST, we evaluated the potential to estimate daily LE and H using satellite LST and global meteorological data. Furthermore, we did not calibrate the LST observations with the *in situ* dataset (Bateni et al., 2013; Bateni and Entekhabi, 2012; Castelli et al., 1999; Xu et al., 2014).

When compared with ground-based measurements (EC) of surface energy balance components, we showed that the estimated H and LE were in agreement with the *in-situ* observations over the study woody savanna site. The mean difference between estimated and observed LE was ~30%, which is in agreement with errors reported in the literature (excluded 2012). These results indicate that assimilating the sequences of Copernicus LST product can partition the available energy between the sensible and latent heat fluxes. The LE and H RMSE values were lower than those reported previously at deciduous forest sites by Xu et al. (2014) using a VDA model. Furthermore, LE RMSE values at 8-days temporal scales (RMSE = 22 W/m²) is lower than the ones reported previously at forest sites when using others schemes to retrieve LE (Barraza et al., 2017; Cleugh et al., 2007; Guerschman et al., 2009; Kalma et al., 2008; Li et al., 2009; Yebra et al., 2013; Zhang et al., 2010). The key advantage of this model is that it provides daily LE and H estimations and not a snapshot like others models that used remote sensing data, or an 8-days composite (Carlson, 2007; Mu et al., 2007; Yebra et al., 2013). Furthermore it does not require extra inputs (like soil moisture), and used only LST as a remote sensing input. However, there are limitations related to: i) LST information at high-resolution (1–3 km) with multiple samples during day, ii) gaps in LST time series, and iii) the need of soil volumetric heat capacity and thermal conductivity as input. To deal with the second limitations (ii) in Section 2.5 we proposed a methodology to fill missing data. However, in relation to (i) the new generation sensors GOES-R and Hamawani 9 will provide data every 15 min with a spatial resolution up to 2 km, improving the availability of data with high spatial resolution. In this context, our study shows the possibility of an operational daily LE estimation scheme using multiple LST observations.

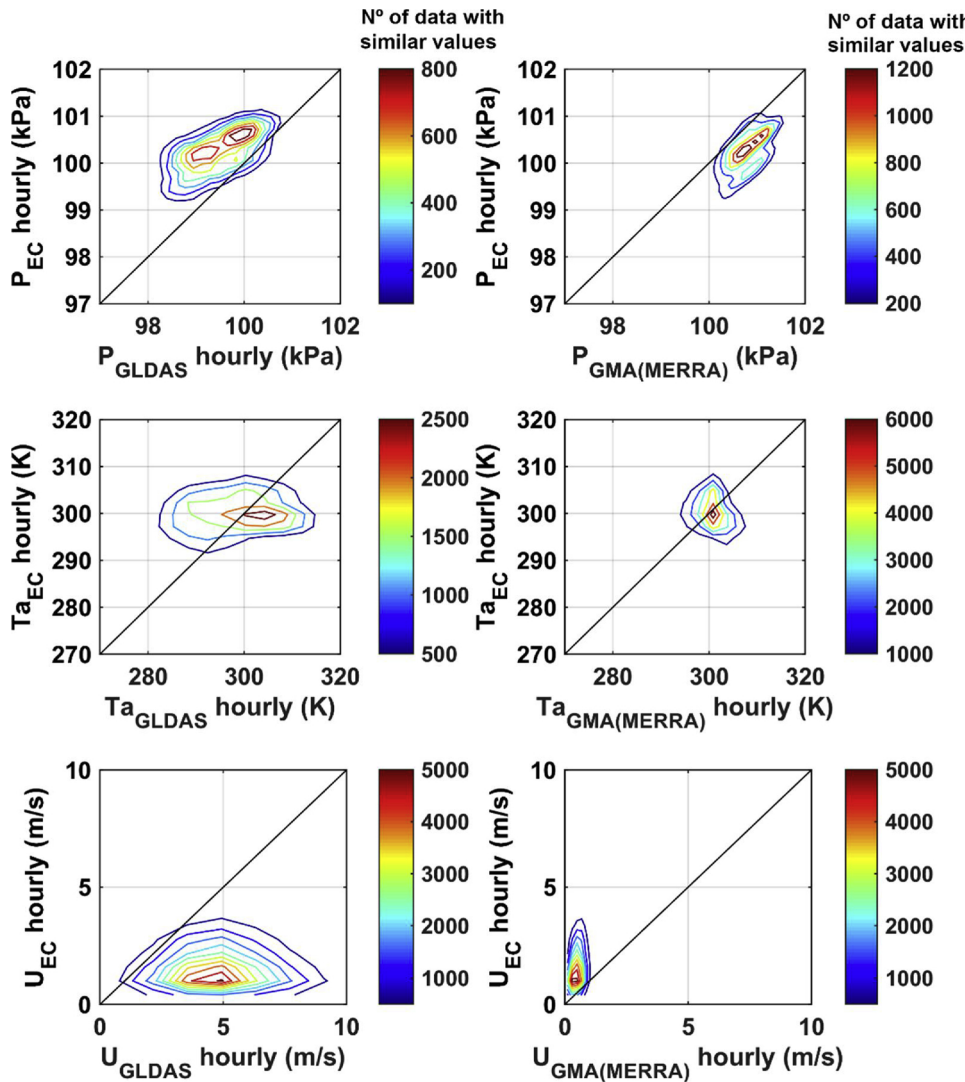


Fig. 6. Relation between Global meteorological data (GMD) and *in-situ* EC meteorological data. The color scale to the right of each plot represents the number of data with similar values. Where GLDAS/NOAH is Global Land Data Assimilation System and GMA/MERRA the Modern Era Retrospective-analysis for Research and Applications.

It is important to mention that at 2012 the CS VDA model underestimate LE with a higher RMSE than for the rest of the time series. The misfits between the model estimates and EC observations were mainly due to error in the LST estimation. In 2012 the effect of the boundaries on EF estimations (EF is constrained to an upper bound of 0.97 and lower bound of 0.1) to avoid numerical instabilities in the model, do not allow the LE and H values to increase as the daytime-average LE and H observations. Xu et al., 2014 found similar result using both the CS and DS VDA models at a grassland ecosystem. Therefore, for all the period analyzed, the errors were related to model assumptions. The C_{HN} parameter is mainly a function of vegetation phenology and is assumed to be constant in each monthly assimilation period (Xu et al., 2016). During the first and the last of stage of the growing season the large variations in LAI violate the assumption of monthly constant C_{HN} and cause underestimations and overestimations of LE and H, respectively (Xu et al., 2016).

Furthermore, EC instrumentation error may have an effect on LE and H estimations (as a second order or importance). All eddy covariance system (EC) and meteorological sensors such as radiation, temperature, and humidity have different footprints. The bias in the EC measurement could be a consequence of energy imbalance. Xu et al., 2014 found that the errors in the estimation of LE using VDA model

were mainly due to problems in the energy balance of the EC data (in his study, the energy balance ratio (LE+H vs Rn-G) was in the range 0.75–0.78). However at HSP, the energy balance ratio (LE+H vs Rn-G) was between 0.89–0.93 during 2010–2015, showing that the EC was able to capture around 90% of the available energy.

At this area, LE is driven primarily by surface meteorology during the rainy season and then there is a strongest control by the vegetation on transpiration during the dry season (reduction of canopy conductance). During the dry season the land surface heterogeneity increase (between soil and vegetation) and therefore the CS model may not represent as well the terrain fluxes. For these reasons the performance of the CS VDA model was better during the rainy season. However, the explained variance were higher than 65% with RMSE values lower than 100 W/m² (excluding 2012).

When evaluating the potential to use GMD as input in the CS-VDA model, we observed the expected degradation of the model performance due to the disagreement between the GMD and *in-situ* meteorological variables. The best result was for the GMA/MERRA dataset. The difference in the performance was due to a better agreement with *in situ* variables of the GMA/MERRA dataset and not due to the different time resolution (GLDAS: 3-hourly and GMA/MERRA: hourly). Part of the disagreement between the reanalysis products and EC observations

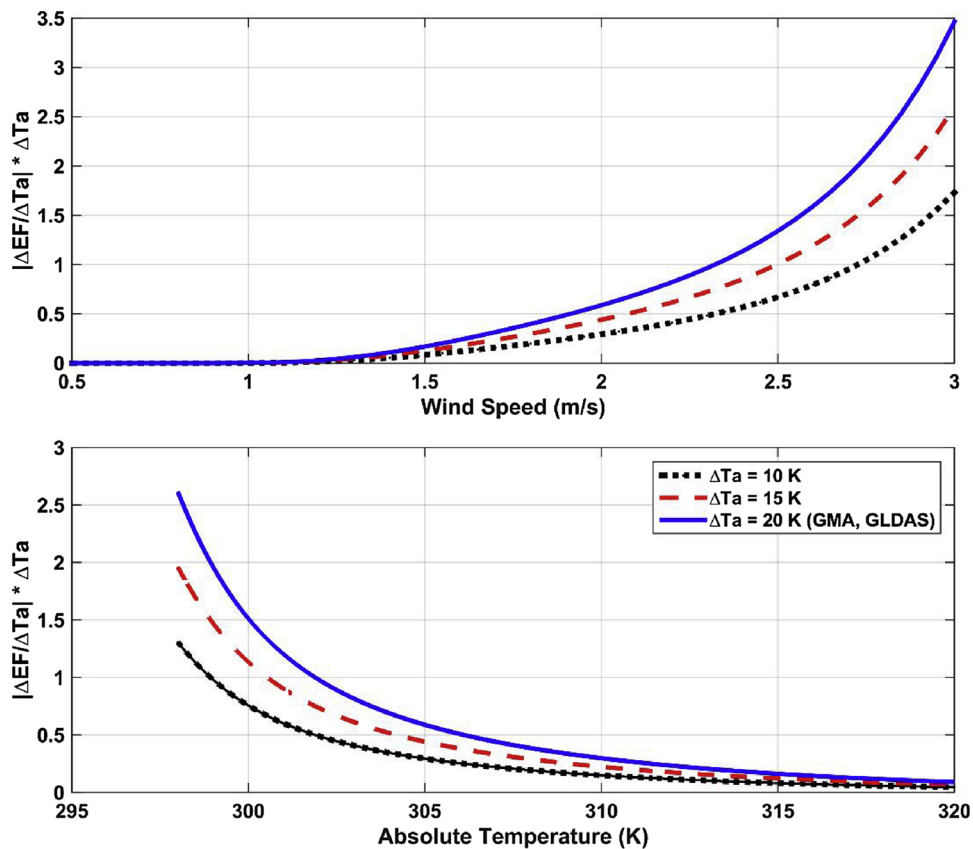


Fig. 7. EF error contribution of Ta ($|\Delta EF / \Delta Ta| \Delta Ta$) as a function of wind speed (U, m/s) (top) and absolute air temperature (Ta, K) (bottom) for different values of ΔTa . Typical value of $\Delta Ta = 20$ K was observed for both GMA (MERRA) and GLDAS for this study site.

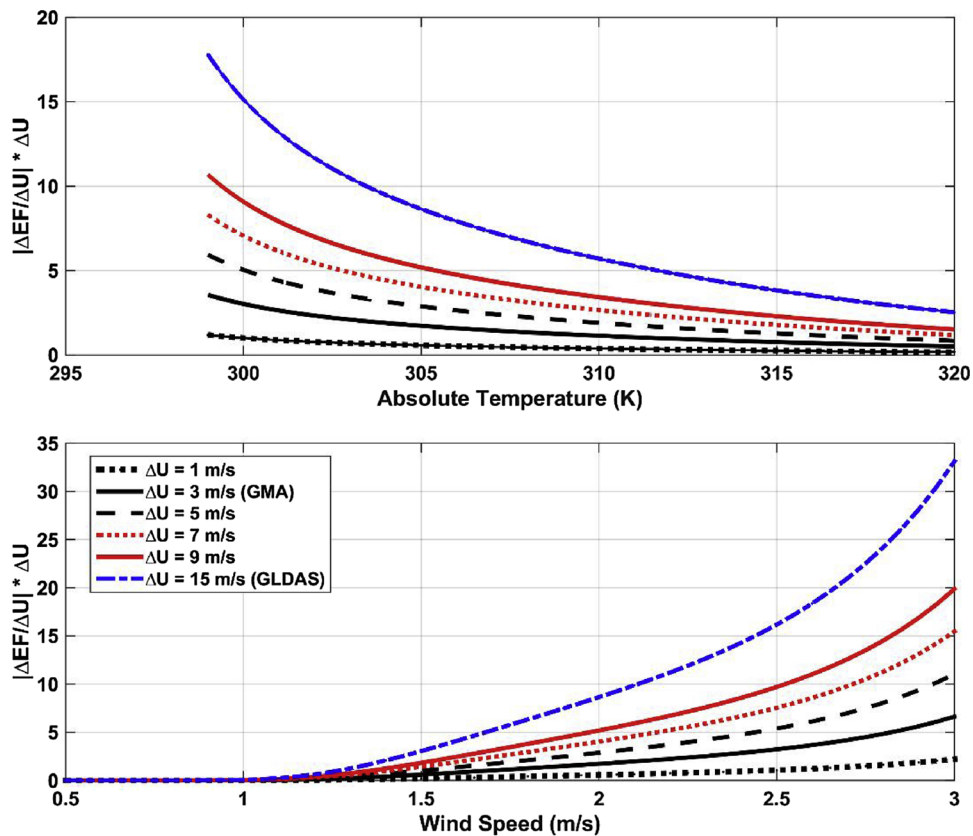


Fig. 8. EF error contribution of U ($|\Delta EF / \Delta U| \Delta U$) as a function of absolute air temperature (Ta, K) (top) and wind speed (U, m/s) (bottom) for different values of ΔU . Typical values of $\Delta U = 3$ m/s (GMA (MERRA)) and $\Delta U = 15$ m/s (GLDAS) for this study site are informed.

is due to the scale differences. The gridded reanalysis products represent the grid-average values of each variable, with the size of a grid box being as large as a few hundred kilometers, while the EC footprint could capture the flux of 1 km around the tower. This is especially important for wind speed with its high spatial and temporal variability.

In general, the error propagation analysis in VDA schemes is not comprehensively studied. In this manuscript, the effect of turbulent heat flux estimations of the uncertainty in air temperature and wind speed (the two key meteorological factors that controls overall estimation error) was quantitatively characterized. This study will be useful to point out the key variables responsible for the increased RMSE errors when using GMD datasets and, to design possible mitigation schemes. In general, it was found that the CS-VDA model is more sensitive to uncertainties in wind speed than in air temperature. Also, the CS-VDA model tends to yield larger errors when fed with large U values. Overall, all of these results clearly demonstrate that the correct specification of meteorological data plays an important role in the accurate retrieval of turbulent heat fluxes. These findings also allow us to quantitatively characterize the effect of uncertainties in replacing *in-situ* for global meteorological data on the turbulent heat flux estimates.

Overall, these results demonstrate several advantages of the CS-VDA model that complement the previous ones found by Bateni et al., 2013; Bateni and Entekhabi, 2012; Xu et al., 2014. Firstly, a 3-h average

meteorological data could be used as input with minor degradation. Secondly, global meteorological data could be used as input (with larger errors). And three, the proposed VDA scheme do not require LST calibration and *in situ* measurement to obtain good results. Despite the fundamentally different approaches (semi-empirical, process-based and variational), CS-VDA and LE products were comparable with existing global product. In particular, LE RMSE values at 8-day temporal scale for the GMD dataset were similar of those reported at this area by MOD16A2 (Mu et al., 2007) and The Breathing Earth System Simulator (BESS (Jiang and Ryu, 2016)) products. We conclude that CS-VDA can serve as a daily estimation of LE and H, and could provide complementary information of flux dynamics than global products (MODIS and BESS). We expect that CS-VDA model could be implemented in other sites with the advance of the new generation sensors GOES-R and Hamawani 9.

Acknowledgments

This work was also funded by PICTO-2014-0099 manejo sustentable de los bosques nativos and GRINGS PIP 2015 N° 899. The author thanks Ozflux Network for making the data freely available as well as the flux tower principal investigators.

Appendix A

The turbulence term could be replaced using the following equation

$$u^* = \frac{k u}{\ln\left(\frac{z-d}{z_0}\right)} \quad (A1)$$

$$r_a = \frac{1}{k^2 u} \ln\left(\frac{z-d}{z_0}\right) \ln\left(\frac{z-d}{z_{OH}}\right) \quad (A2)$$

$$G_a = \frac{1}{r_a} \quad (A3)$$

where U is the surface mean wind speed (m/s) measured height (z) (s/m), r_a is the aerodynamic resistance (s/m); u^* is friction velocity (m/s); d the zero-plane displacement and, z_0 and z_{OH} the roughness lengths for momentum and heat respectively (m). The quantities d, z_0 and z_{OH} were estimated as $d = 2 h/3$, 0.123 h and 0.0123 h respectively, where h is canopy height (14 m).

References

- Allen, R.G., Pereira, L.S., Raes, D., Smith, M., et al., 1998. Crop Evapotranspiration—Guidelines for Computing Crop Water Requirements—FAO Irrigation and drainage paper 56 300. FAO, Rome, pp. 6541.
- Barraza, V., Restrepo-Coupe, N., Huete, A., Grings, F., Van Gorsel, E., 2015. Passive microwave and optical index approaches for estimating surface conductance and evapotranspiration in forest ecosystems. Agric. For. Meteorol. 213, 126–137. <https://doi.org/10.1016/j.agrformet.2015.06.020>.
- Barraza, V., Restrepo-Coupe, N., Huete, A., Grings, F., Beringer, J., Cleverly, J., Eamus, D., 2017. Estimation of latent heat flux over savannah vegetation across the North Australian Tropical Transect from multiple sensors and global meteorological data. Agric. For. Meteorol. 232, 689–703. <https://doi.org/10.1016/j.agrformet.2016.10.013>.
- Bateni, S.M., Entekhabi, D., 2012. Relative efficiency of land surface energy balance components. Water Resour. Res. 48, W04510. <https://doi.org/10.1029/2011WR011357>.
- Bateni, S.M., Entekhabi, D., Jeng, D.-S., 2013. Variational assimilation of land surface temperature and the estimation of surface energy balance components. J. Hydrol. (Amst) 481, 143–156. <https://doi.org/10.1016/j.jhydrol.2012.12.039>.
- Bohren, C.F., Albrecht, B.A., 1998. Atmospheric Thermodynamics, Edición: New. ed. OUP USA, New York.
- Boussetta, S., Koike, T., Yang, K., Graf, T., Pathmathevan, M., 2008. Development of a coupled land-atmosphere satellite data assimilation system for improved local atmospheric simulations. Remote Sens. Environ. 112, 720–734. <https://doi.org/10.1016/j.rse.2007.06.002>.
- Carlson, T., 2007. An overview of the “Triangle method” for estimating surface evapotranspiration and soil moisture from satellite imagery. Sensors 7, 1612–1629. <https://doi.org/10.3390/s7081612>.
- Castelli, F., Entekhabi, D., Caporali, E., 1999. Estimation of surface heat flux and an index of soil moisture using adjoint-state surface energy balance. Water Resour. Res. 35,
- 3115–3125.
- Cleugh, H.A., Leuning, R., Mu, Q., Running, S.W., 2007. Regional evaporation estimates from flux tower and MODIS satellite data. Remote Sens. Environ. 106, 285–304. <https://doi.org/10.1016/j.rse.2006.07.007>.
- Crow, W.T., Kustas, W.P., 2005. Utility of assimilating surface radiometric temperature observations for evaporative fraction and heat transfer coefficient retrieval. Bound.-Layer Meteorol. 115, 105–130. <https://doi.org/10.1007/s10546-004-2121-0>.
- Gillies, R.R., Kustas, W.P., Humes, K.S., 1997. A verification of the ‘triangle’ method for obtaining surface soil water content and energy fluxes from remote measurements of the Normalized Difference Vegetation Index (NDVI) and surface e. Int. J. Remote Sens. 18, 3145–3166.
- Guerschman, J.P., Van Dijk, A.I.J.M., Mattersdorf, G., Beringer, J., Hutley, L.B., Leuning, R., Pipunic, R.C., Sherman, B.S., 2009. Scaling of potential evapotranspiration with MODIS data reproduces flux observations and catchment water balance observations across Australia. J. Hydrol. (Amst) 369, 107–119. <https://doi.org/10.1016/j.jhydrol.2009.02.013>.
- Hu, Z., Islam, S., 1995. Prediction of ground surface temperature and soil moisture content by the force-restore method. Water Resour. Res. 31, 2531–2539. <https://doi.org/10.1029/95WR01650>.
- Huntingford, C., Hugo Lambert, F., Gash, J.H., Taylor, C.M., Challinor, A.J., 2005. Aspects of climate change prediction relevant to crop productivity. Philos. Trans. R. Soc. B Biol. Sci. 360, 1999–2009. <https://doi.org/10.1098/rstb.2005.1748>.
- Hutley, L.B., Beringer, J., Isaac, P.R., Hacker, J.M., Cernusak, L.A., 2011. A sub-continent scale living laboratory: spatial patterns of savanna vegetation over a rainfall gradient in northern Australia. Agric. For. Meteorol. 151, 1417–1428. <https://doi.org/10.1016/j.agrformet.2011.03.002>.
- Isaac, P., Cleverly, J., McHugh, I., van Gorsel, E., Ewenz, C., Beringer, J., 2017. OzFlux data: network integration from collection to curation. Biogeosciences 14, 2903–2928. <https://doi.org/10.5194/bg-14-2903-2017>.
- Jensen, N.O., Hummelshøj, P., 1995. Derivation of canopy resistance for water vapour fluxes over a spruce forest, using a new technique for the viscous sublayer resistance. Agric. For. Meteorol., Biospheric Aspects of the Hydrological Cycle 73, 339–352.

- [https://doi.org/10.1016/0168-1923\(94\)05083-I](https://doi.org/10.1016/0168-1923(94)05083-I).
- Jiang, C., Ryu, Y., 2016. Multi-scale evaluation of global gross primary productivity and evapotranspiration products derived from Breathing Earth System Simulator (BESS). *Remote Sens. Environ.* 186, 528–547. <https://doi.org/10.1016/j.rse.2016.08.030>.
- Kalma, J.D., McVicar, T.R., McCabe, M.F., 2008. Estimating land surface evaporation: a review of methods using remotely sensed surface temperature data. *Surv. Geophys.* 29, 421–469. <https://doi.org/10.1007/s10712-008-9037-z>.
- Kalnay, E., Kanamitsu, M., Kistler, R., Collins, W., Deaven, D., Gandin, L., Iredell, M., Saha, S., White, G., Woollen, J., Zhu, Y., Leetmaa, A., Reynolds, R., Chelliah, M., Ebisuzaki, W., Higgins, W., Janowiak, J., Mo, K.C., Ropelewski, C., Wang, J., Jenne, R., Joseph, D., 1996. The NCEP/NCAR 40-Year reanalysis project. *Bull. Am. Meteorol. Soc.* 77, 437–471. [https://doi.org/10.1175/1520-0477\(1996\)077<437:TNYRP>2.0.CO;2](https://doi.org/10.1175/1520-0477(1996)077<437:TNYRP>2.0.CO;2).
- Kanniah, K.D., Beringer, J., Hutley, L., 2011. Exploring the link between clouds, radiation, and canopy productivity of tropical savannas. *Agric. For. Meteorol.* <https://doi.org/10.1016/j.agrformet.2013.06.010>.
- Kottek, M., Grieser, J., Beck, C., Rudolf, B., Rubel, F., 2006. World Map of the Köppen-Geiger climate classification updated. *Meteorol. Z.* 259–263. <https://doi.org/10.1127/0941-2948/2006/0130>.
- Li, R., Min, Q., Lin, B., 2009. Estimation of evapotranspiration in a mid-latitude forest using the Microwave Emissivity Difference Vegetation Index (EDVI). *Remote Sens. Environ.* 113, 2011–2018. <https://doi.org/10.1016/j.rse.2009.05.007>.
- Liu, D., Song, K., Townsend, J.R.G., Gong, P., 2008. Using local transition probability models in Markov random fields for forest change detection. *Remote Sens. Environ.* 112, 2222–2231. <https://doi.org/10.1016/j.rse.2007.10.002>.
- McNaughton, K.G., Van Den Hurk, B.J.M., 1995. A 'Lagrangian' revision of the resistors in the two-layer model for calculating the energy budget of a plant canopy. *Bound.-Layer Meteorol.* 74, 261–288. <https://doi.org/10.1007/BF00712121>.
- Monteith, J.L., 1985. Evaporation from land surfaces: progress in analysis and prediction since 1948. *Advances in Evapotranspiration. Presented at the Proceedings of the ASAE Conference on Evapotranspiration 4-12*.
- Moran, M.S., Jackson, R.D., 1991. Assessing the spatial distribution of evapotranspiration using remotely sensed inputs. *J. Environ. Qual.* 20, 725. <https://doi.org/10.2134/jeq1991.00472425002000040003x>.
- Mu, Q., Heinisch, F.A., Zhao, M., Running, S.W., 2007. Development of a global evapotranspiration algorithm based on MODIS and global meteorology data. *Remote Sens. Environ.* 111, 519–536. <https://doi.org/10.1016/j.rse.2006.07.007>.
- Nagler, P.L., Scott, R.L., Westenbrug, C., Cleverly, J.R., Glenn, E.P., Huete, A.R., 2005. Evapotranspiration on western US rivers estimated using the enhanced vegetation index from MODIS and data from eddy covariance and Bowen ratio flux towers. *Remote Sens. Environ.* 97, 337–351.
- Oke, T.R., 1988. *Boundary Layer Climates*, 2nd ed. Routledge, London.
- Restrepo-Coupe, N., da Rocha, H.R., Hutyra, L.R., da Araujo, A.C., Borma, L.S., Christoffersen, B., Cabral, O.M.R., de Camargo, P.B., Cardoso, F.L., da Costa, A.C.L., Fitzjarrald, D.R., Goulden, M.L., Kruijt, B., Maia, J.M.F., Malhi, Y.S., Manzi, A.O., Miller, S.D., Nobre, A.D., von Randow, C., Sá, L.D.A., Sakai, R.K., Tota, J., Wofsy, S.C., Zanchi, F.B., Saleska, S.R., 2013. What drives the seasonality of photosynthesis across the Amazon basin? A cross-site analysis of eddy flux tower measurements from the Brasil flux network. *Agric. For. Meteorol.* 182–183, 128–144. <https://doi.org/10.1016/j.agrformet.2013.04.031>.
- Restrepo-Coupe, N., Huete, A., Davies, K., Cleverly, J., Beringer, J., Eamus, D., van Gorsel, E., Hutley, L.B., Meyer, W.S., 2015. MODIS vegetation products as proxies of photosynthetic potential: a look across meteorological and biologic driven ecosystem productivity. *Biogeosci. Discuss.* 12, 19213–19267. <https://doi.org/10.5194/bgd-12-19213-2015>.
- Rodell, M., Houser, P.R., Jambor, U., Gottschalck, J., Mitchell, K., Meng, C.-J., Arsenault, K., Cosgrove, B., Radakovich, J., Bosilovich, M., Entin, J.K., Walker, J.P., Lohmann, D., Toll, D., 2004. The global land data assimilation system. *Bull. Am. Meteorol. Soc.* 85, 381–394. <https://doi.org/10.1175/BAMS-85-3-381>.
- Ryu, Y., Baldocchi, D.D., Kobayashi, H., van Ingen, C., Li, J., Black, T.A., Beringer, J., van Gorsel, E., Knohl, A., Law, B.E., Roupsard, O., 2011. Integration of MODIS land and atmosphere products with a coupled-process model to estimate gross primary productivity and evapotranspiration from 1 km to global scales. *Glob. Biogeochem. Cycles* 25. <https://doi.org/10.1029/2011GB004053>. GB4017.
- Sabater, J.M., Jarlan, L., Calvet, J.-C., Bouyssel, F., De Rosnay, P., 2007. From near-surface to root-zone soil moisture using different assimilation techniques. *J. Hydrometeorol.* 8, 194–206. <https://doi.org/10.1175/JHM571.1>.
- Schubert, S.D., Rood, R.B., Pfaendtner, J., 1993. An assimilated dataset for earth science applications. *Bull. Am. Meteorol. Soc.* 74, 2331–2342. [https://doi.org/10.1175/1520-0477\(1993\)074<2331:AADFES>2.0.CO;2](https://doi.org/10.1175/1520-0477(1993)074<2331:AADFES>2.0.CO;2).
- Taylor, J.A., Tulloch, D., 1985. Rainfall in the wet-dry tropics: extreme events at Darwin and similarities between years during the period 1870–1983 inclusive. *Aust. J. Ecol.* 10, 281–295. <https://doi.org/10.1111/j.1442-9993.1985.tb00890.x>.
- Xu, T., Bateni, S.M., Liang, S., Entekhabi, D., Mao, K., 2014. Estimation of surface turbulent heat fluxes via variational assimilation of sequences of land surface temperatures from Geostationary Operational Environmental Satellites. *J. Geophys. Res. Atmos.* 119 (2014), JD021814. <https://doi.org/10.1002/2014JD021814>.
- Xu, T., Bateni, S.M., Margulis, S.A., Song, L., Liu, S., Xu, Z., 2016. Partitioning evapotranspiration into soil evaporation and canopy transpiration via a two-source variational data assimilation system. *J. Hydrometeorol.* 17, 2353–2370. <https://doi.org/10.1175/JHM-D-15-0178.1>.
- Yebra, M., Dennison, P.E., Chuvieco, E., Riaño, D., Zylstra, P., Hunt, E.R., Danson, F.M., Qi, Y., Jurdao, S., 2013. Remote Sensing of Environment A global review of remote sensing of live fuel moisture content for fire danger assessment : Moving towards operational products. *Remote Sens. Environ.* 136, 455–468. <https://doi.org/10.1016/j.rse.2013.05.029>.
- Zhang, K., Kimball, J.S., Nemani, R.R., Running, S.W., 2010. A continuous satellite-derived global record of land surface evapotranspiration from 1983 to 2006. *Water Resour. Res.* 46, W09522. <https://doi.org/10.1029/2009WR008800>.